Forest Ecology and Management 419–420 (2018) 291–304

Contents lists available at ScienceDirect

Forest Ecology and Management

journal homepage: www.elsevier.com/locate/foreco

Landscape-scale variation in canopy water content of giant sequoias during drought☆

Tarin Paz-Kagan[a,*], Nicholas R. Vaughn[a], Roberta E. Martin[a], Philip G. Brodrick[a], Nathan L. Stephenson[b], Adrian J. Das[b], Koren R. Nydick[c], Gregory P. Asner[a]

[a] Department of Global Ecology, Carnegie Institution for Science, Stanford, CA 94305, USA
[b] U.S. Geological Survey, Western Ecological Research Center, Three Rivers, CA 93271, USA
[c] Sequoia and Kings Canyon National Parks, Three Rivers, CA 93271, USA

ARTICLE INFO

Keywords:
Foliage status
Carnegie Airborne Observatory
Climate change
Imaging spectroscopy
Sequoia and Kings Canyon National Parks (SEKI)

ABSTRACT

Recent drought (2012–2016) caused unprecedented foliage dieback in giant sequoias (*Sequoiadendron giganteum*), a species endemic to the western slope of the southern Sierra Nevada in central California. As part of an effort to understand and map sequoia response to droughts, we studied the patterns of remotely sensed canopy water content (CWC), both within and among sequoia groves in two successive years during the drought period (2015 and 2016). Our aims were: (1) to quantify giant sequoia responses to severe drought stress at a landscape scale using CWC as an indicator of crown foliage status, and (2) to estimate the effect of environmental correlates that mediate CWC change within and among giant sequoia groves. We utilized airborne high fidelity imaging spectroscopy (HiFIS) and light detection and ranging (LiDAR) data from the Carnegie Airborne Observatory to assess giant sequoia foliage status during 2015 and 2016 of the 2012–2016 droughts. A series of statistical models were generated to classify giant sequoias and to map their location in Sequoia and Kings Canyon National Parks (SEKI) and vicinity. We explored the environmental correlates and the spatial patterns of CWC change at the landscape scale. The mapped CWC was highly variable throughout the landscape during the two observation years, and proved to be most closely related to geological substrates, topography, and site-specific water balance. While there was an overall net gain in sequoia CWC between 2015 and 2016, certain locations (lower elevations, steeper slopes, areas more distant from surface water sources, and areas with greater climate water deficit) showed CWC losses. In addition, we found greater CWC loss in shorter sequoias and those growing in areas with lower sequoia stem densities. Our results suggest that CWC change indicates sequoia response to droughts across landscapes. Long-term monitoring of giant sequoia CWC will likely be useful for modeling and predicting their population-level response to future climate change.

1. Introduction

California experienced its most severe drought in more than a century between the years 2012 and 2016, characterized by historically low precipitation combined with particularly warm temperatures and forest insect outbreaks (Diffenbaugh et al., 2015; Swain et al., 2016). These factors generated a large pulse of canopy water loss and tree mortality throughout the state (Asner et al., 2016a; Young et al., 2017). In addition, the ongoing drought generated a severe reduction in soil moisture, groundwater levels, and reservoir stocks (Diffenbaugh et al., 2015). One area that experienced extensive drought stress was the Sierra Nevada region, which had undergone a dramatic decline in winter snowpack and an increase in the length of the summer drought period (Griffin and Anchukaitis, 2014). Large-scale tree mortality was observed throughout the Sierra Nevada, with observations of millions of dead trees (Asner et al., 2016a; Young et al., 2017). During the third year of the drought (2014), giant sequoias (*Sequoiadendron giganteum*) exhibited foliage dieback (Stephenson et al., this issue). As a result, there has been a growing concern regarding giant sequoia responses to drought stress.

Giant sequoias are endemic to the western Sierra Nevada, are generally confined to a narrow mid-elevation range (1400–2150 m), and are restricted to roughly 70 groves that occupy about 14,600 ha (Stephenson, 1999). Giant sequoias are the most massive tree species on

☆ This article is part of a special feature entitled "Leaf to landscape responses of giant sequoia to hotter drought", published in the Journal of Forest Ecology and Management 419–420, 2018.

* Corresponding author.
E-mail addresses: tpazkagan@carnegiescience.edu, tarin@volcani.agri.gov.il (T. Paz-Kagan).

https://doi.org/10.1016/j.foreco.2017.11.018
Received 23 August 2017; Received in revised form 30 October 2017; Accepted 7 November 2017
Available online 20 November 2017
0378-1127/ © 2017 Elsevier B.V. All rights reserved.

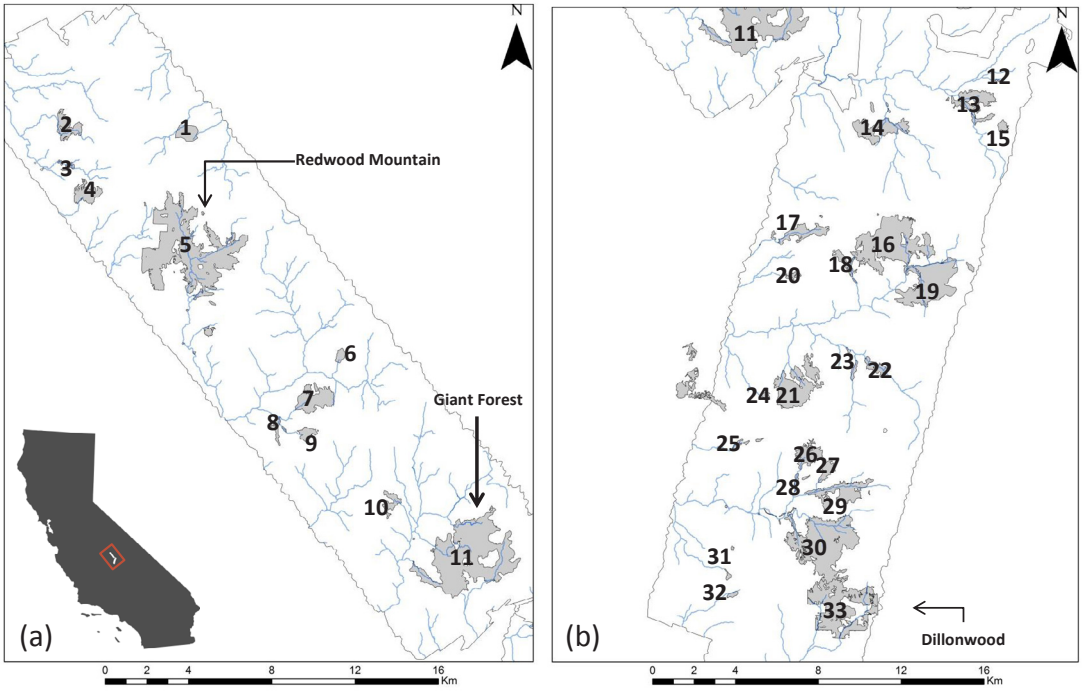

Fig. 1. (a) Carnegie Airborne Observatory (CAO) flight coverage throughout 33 giant sequoia groves and aggregated groves (small groves adjacent to each other) in the northern (a) and the southern areas (b) on the western slope of the southern Sierra Nevada in central California, together with the grove map and rivers and streams. Grove numbers correspond to those in Table 4.

earth, among the tallest, reaching heights of up to 95 m, and among the oldest, sometimes having a life span of 3200 years or longer (Stephenson, 1996; York et al., 2011). Giant sequoias are known for their remarkable pest, pathogen, and fire resistance (Hartesveldt et al., 1975), and their present species range appears to be based on abundant soil moisture (Rundel, 1972).

Giant sequoias deploy multiple adaptation strategies to cope with water stress, including shoot and leaf succulence, leaf toughness, and optimization for heat accumulation in the transpiration tissues (Ambrose et al., 2016). The ability of giant sequoias to tolerate water stress is possible, in part, because its leaves are responsive to environmental change. Chin and Sillett (2016) have shown that phenotypic plasticity allows giant sequoias to adapt their foliage to within-crown environments, maximizing limited windows of stomatal openness through rapid hydraulic throughput and resistance to water stress-induced damage. Additional adaptations to cope with water stress in giant sequoias have been found, including tight stomatal control of water loss and increasing xylem cavitation resistance with height (Ambrose et al., 2015; Ambrose et al., this issue). These findings provide insight into the isohydric approach through which giant sequoias regulate their stomatal conductance, transpiration, and resultant water loss rates (Tardieu and Simonneau, 1998). Isohydric trees regulate stomatal conditions to maintain minimum water potential within a relatively narrow range, thereby reducing the risk of damaging xylem cavitation (Roman et al., 2015). However, this strategy causes them to close their stomata in response to even mild water stress, which reduces carbon uptake.

While our knowledge about physiological responses to drought at the leaf and whole tree level is growing, the understanding of crown-level responses in giant sequoias at local (grove) to a regional scale still remains a challenge. Ground-based measurements provide insight into the mechanisms of drought responses in trees, but are often limited to relatively few individuals, especially in trees of tall stature such as giant sequoias. These measurements are expensive and time-consuming, and thus cannot meet the requirements of landscape-scale assessment and management. Remote sensing offers a means to measure the canopy condition of a large number of trees, which may provide insight into whether giant sequoias are responding at the canopy and/or landscape level. Remote sensing technologies, such as high fidelity imaging spectroscopy (HiFIS) and light detection and ranging (LiDAR) measurements, may improve our understanding of giant sequoia responses to drought stressors at landscape scales. The combination of high spatial and spectral resolutions provided by HiFIS is particularly suitable for this task, providing a powerful technique for mapping specific species at the crown level, based on the reflectance properties of tree canopies (Asner and Martin, 2015; Asner et al., 2015; Baldeck et al., 2015). HiFIS can also be used to study foliage status as part of the trees' physiological and biophysical status (Asner et al., 2014; Asner et al., 2015). The LiDAR data can be used to study the giant sequoia's responses to environmental control via both topographic characteristics and canopy characteristics such as top-of-canopy height above ground (Omasa et al., 2007).

One of the most applied HiFIS measurements of foliage status is canopy water content (CWC), which is defined as the total amount of liquid water in the foliage of a canopy expressed in $L\,m^{-2}$ (Asner et al., 2004; Farooq et al., 2009). CWC is broadly correlated with the combination of leaf water content and leaf area index, thus serving as an indicator of progressive drought-related stress (Ustin et al., 1998; Cheng et al., 2006; Asner et al., 2016a). Martin et al. (this issue) combined the airborne HiFIS remote sensing measurements taken in 2015 and 2016 to assess the biophysical responses of giant sequoias to drought. In 49 studied trees, CWC was related to leaf water potential in both years and non-structural carbohydrates (NSC, %) in one year, but not to other foliar traits including leaf water content, leaf mass per area ($g\,m^{-2}$), foliar δ13C, and total nitrogen (%) suggesting that changes in CWC were made at the whole-canopy rather than the leaf scale. Martin et al. (this issue) detected a clear relationship between CWC and foliage dieback, even without taking into account new or prior variability in leaf growth. This connection between CWC and foliage dieback suggests that CWC of giant sequoias might serve as an indicator of water stress in giant sequoia canopies using HiFIS. In particular, foliage dieback was most likely a controlled process of drought-induced senescence and not

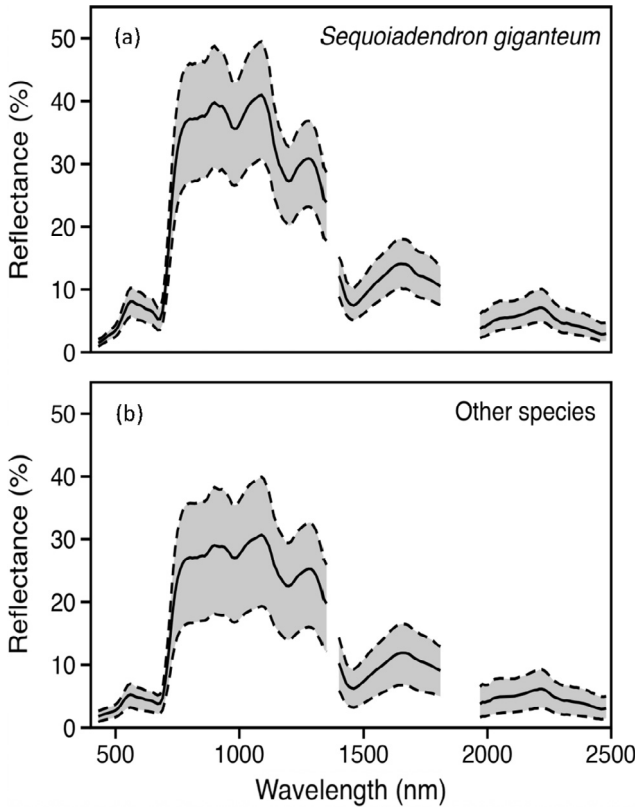

Fig. 2. Mean and 95% confidence intervals for top of canopy reflectance spectra from (a) pixels in the giant sequoia class, and (b) "other trees" pixels from other conifer tree species. Portions of the spectrum where atmospheric water interferes with the measurement have been removed.

the direct effects of hydraulic failure (Stephenson et al., this issue).

Understanding how drought stress affects giant sequoias at the landscape scale is critical for modeling and predicting their population-level responses to drought and other climatic changes (Jump et al., 2009; Jump et al., 2010). Here we focused on 33 giant sequoia groves or aggregated groves (small groves adjacent to each other), located throughout Sequoia and Kings Canyon National Park (SEKI) and vicinity in the western Sierra Nevada of California (Fig. 1). We used airborne HiFIS and LiDAR data from the Carnegie Airborne Observatory (Asner et al., 2012) to quantify giant sequoia CWC change between 2015 and 2016, at the end of the 2012–2016 drought. In addition, we studied environmental correlates of CWC variation both within and among sequoia groves. Specifically, we asked the following questions: (1) how does CWC in giant sequoias vary across the landscape (within and among groves)?; (2) what were the environmental correlates of 2015–2016 CWC change in giant sequoias?; (3) what can the patterns of these responses tell us about giant sequoia susceptibility and resilience to future droughts at the landscape scale of groves located throughout Sequoia and Kings Canyon National Parks (SEKI)?

2. Methodology

2.1. Study system

In the current study, 33 giant sequoia groves and aggregated groves (small groves adjacent to each other) were mapped and studied in SEKI and vicinity (Fig. 1), with a total grove area of 5782.51 ha. The giant sequoia groves are located in a Mediterranean climate region, with the mean annual temperature declining relatively steeply with elevation, from 12 °C at 1400 m elevation (near the lower treeline, upper chaparral, and woodland limits) to 1 °C at 3400 m (near the upper treeline) (Fites-Kaufman et al., 2007). Mean annual precipitation ranges from 1000 to 1400 mm year^{-1}. At the elevations at which sequoia groves are found, roughly one half of annual precipitation falls as snow. The sequoia groves tend to occur on sites with more available soil moisture than the surrounding forest (Rundel, 1972; Stephenson, 1996). The soil in the area is relatively young (Inceptisols soil taxonomy). In the groves, giant sequoias are accompanied by various tree species, with white fir (*Abies concolor*) and sugar pine (*Pinus lambertiana*) being the most common, leading to the characterization of the groves as a mixed conifer forest (Meyer and Safford, 2011).

2.2. Remote sensing data collection

In August 2015 and July 2016, HiFIS and LiDAR data were collected using the Carnegie Airborne Observatory over two areas, hereafter referred to as the north and south areas (Fig. 1), encompassing the Giant Forest and 32 other giant sequoia groves or aggregated groves (small groves adjacent to each other). The HiFIS spectral radiance data spanned a wavelength range of 350–2480 nm in 427 bands at 5 nm bandwidth, which were later convolved to 214 channels of 10-nm bandwidth in order to reduce data volume, at a 2.0 m ground pixel size resolution. The LiDAR data also had a resolution of 2.0 m, interpolated to a raster digital elevation model (DEM) for the ground surface and digital surface model (DSM), using the LAStools software package (Rapidlasso, GmbH, Gilching, Germany). Measurement of the vertical differences between the DEM and DSM yielded the digital canopy model (DCM) of top-of-canopy height (TCH). The spectral data were filtered using a LiDAR and HiFIS fusion technique to remove bare-ground and shaded canopies by incorporating 3D LiDAR information as described by Asner et al. (2012). Additional information on the remote sensing data collection, image processing, and the LiDAR and HiFIS data fusion technique are described in Martin et al. (this issue).

2.3. Mapping giant sequoias

To estimate the effects of environmental factors on giant sequoia CWC at the grove level, we first needed to isolate giant sequoia locations from other trees within the groves. The spectral reflectance of giant sequoia trees was distinctly different from those of other species, thus facilitating the use of HiFIS data for the purpose of mapping giant sequoias throughout the landscape (Fig. 2). HiFIS measures the spectral radiance reflected from the land surface in narrow, overlapping, and contiguous spectral channels (Lee et al., 2015). After compensation for illumination and atmospheric effects, HiFIS-measured spectral reflectance yields quantitative measurements of the mass-concentration of biologically important molecules and elements (Clark et al., 2003; Serbin et al., 2014; Asner et al., 2015), some of which are diagnostic and predictive for species mapping. The spectral differences in the signature reflectance of giant sequoias compared to other tree species are related to overlap among and within the spectral variability that are related to their unique biological properties. More specifically, these difference in the spectral signal are related to the amplitude and the spectral angle (Féret and Asner, 2013), raising the feasibility of giant sequoia species identification. HiFIS and LiDAR imagery were combined with field sampling data and used to train a gradient boosting machine (GBM) algorithm (Friedman, 2001) to classify giant sequoias and thereby quantify the spatial extent of giant sequoias crowns. The classification was based on two classes: (1) giant sequoia, and (2) "other trees" species.

Giant sequoia crowns used to train the GBM were identified using a variety of data sources. First, 49 giant sequoia trees in the Giant Forest were identified through field work using 2015 HiFIS imagery on a tablet PC integrated with a differentially corrected Global Positioning System. To increase the number of sequoia crowns for our study, we used three additional sources of information on giant sequoia location: (1) a shapefile of giant sequoia groves provided by the National Park Service (NPS), (2) a Google Earth image to identify the giant sequoia

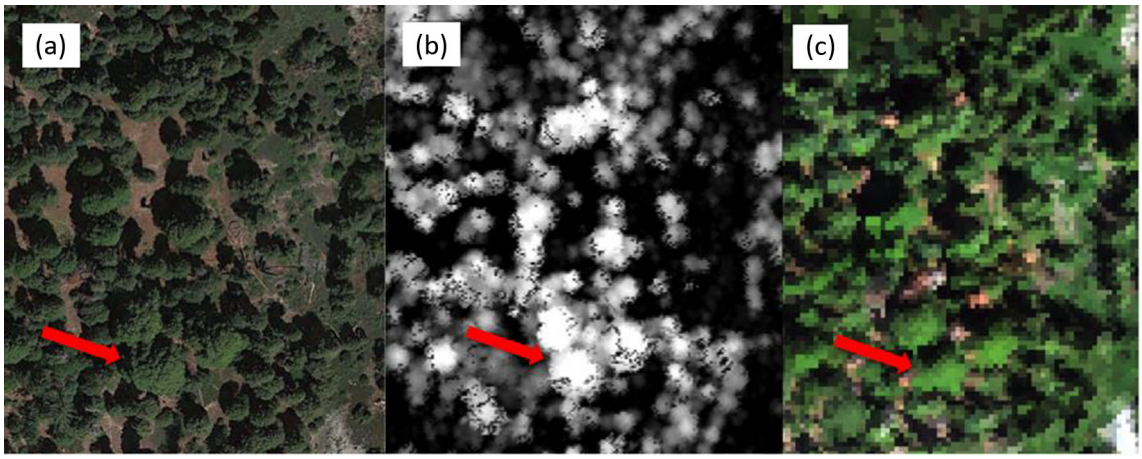

Fig. 3. Example of the use of imagery from Google earth (a), LiDAR canopy height data (b), and high fidelity imaging spectroscopy (HiFIS) reflectance data (RGB composite) used to identify giant sequoia pixels to train the gradient boosting machine model (c).

Table 1
The number of crowns and pixels that were used to train of the gradient boosting machine (GBM) classification model.

		Number of crowns	Number of pixels
North area	Giant sequoia	258	1534
	Other trees	258	4287
South area	Giant sequoia	130	1534
	Other trees	122	2927
Total		719	10282

crowns that were differentiable from other tree species based on color and shape, and (3) a LiDAR TCH image to identify the tallest trees above 50 m. Fig. 3 shows an example of how we used these three data sources to identify giant sequoia pixels to train the GBM classification model. Overall, we identified 258 and 130 giant sequoia crowns in the northern and southern landscapes, respectively, for a total of 388 crowns as focal class training for the GBM classification model (Table 1). The "other trees" class was manually selected from areas in the HiFIS image that were not located within NPS-grove designated areas, and were situated outside of the giant sequoia groves. We identified 258 and 122 additional tree crowns in the north and south images as "other trees" for a total of 380 crowns as training for the GBM classification model. The selected areas were then extracted from the HiFIS image and used to develop a giant sequoia classification map.

We used GBM classification, which is a machine learning technique that produces a prediction model based on ensembles of decision trees (Friedman, 2001). We selected GBM classification because it accommodates complex nonlinear interactions in datasets with collinearity within the predictor variables, as well as different types of variables with non-normal distributions, and because it handles missing values and non-independent data (Friedman and Meulman, 2003). The GBM classification model was constructed using model performances of a 10-fold cross-validation between the calibration and the validation sets, which used 90% of the data as the training set, to develop the model, with the remaining 10% of the data set aside as a test set to examine the accuracy of the model. We selected meta-parameters (the tree complexity/depth, the learning rate, and the number of trees) that maximized the validation set area under the curve (AUC), while still maintaining a reasonable computation time (Elith et al., 2008). AUC is a commonly used measure of model performance, calculated as the integral under the true positive rate versus false positive rate tradeoff curve, also known as the receiver operating characteristic (ROC) curve. The analyses were conducted in the machine learning platform H2O with a Python interface (Baldominos et al., 2014). After training, we applied the model to the HiFIS image to generate a pixel classification of 'sequoia' or 'other trees' across the landscape.

Due to the structural complexity of giant sequoia crowns, attempted LiDAR-based crown-segmentation produced crown sizes that were too small to be realistic. Since a single giant sequoia tree generally occupies more than one pixel, we use a series of three heuristically-based kernel filters to remove spurious pixels with a positive sequoia identification that were likely to be false positives. The first kernel switched the class from 'sequoia' to 'other trees' of any pixel where less than 4 pixels within a 5 × 5 window centered on the target pixel were identified as sequoias. The second and third filters worked essentially the same, but with the second filter using a 7 × 7 window and requiring less than 10 'sequoia' pixels, and the third using a 3 × 3 window and requiring less than 4 'sequoia' pixels. These thresholds were selected through careful examination of the resulting image, and were based on the general size of sequoia crowns as well as the stand-based nature of sequoia growth. In addition, we limited the mapped giant sequoia crowns to the NPS-grove boundaries.

2.4. Landscape canopy water content and change

Calculations of canopy water content (CWC) were conducted using the methods of Asner et al. (2012, 2016a, 2016b) and are described in Martin et al. (this issue). Maps of CWC for 2015 and 2016 were developed from the HiFIS and LiDAR data. The CWC change was calculated as the absolute change (L m^{-2}) from 2015 to 2016 (i.e., 2016 CWC minus 2015 CWC) and the proportional change was calculated as the absolute change in CWC divided by 2015 CWC, meaning positive values indicate a gain in CWC and negative values a reduction in the CWC. The absolute and proportional changes generally showed similar pattern and trend ($R^2 = 0.98$, $p \leq 0.01$) in our study. A similar pattern was demonstrated in CWC of coniferous forest in California by Brodrick and Asner (2017). Prior to the calculation of CWC change, shade filtering was performed on both the 2015 and 2016 CWC maps, as in Asner et al. (2012), so that the images from both years would represent fully sunlight-exposed giant sequoia crowns. By combining HiFIS measurements with 3D forest imaging via LiDAR scanning, we excluded non-forest canopies, such as grasses and short shrubs, as well as bare ground, rock cover, and infrastructure, from the intended measurement using a 10 m LiDAR-driven TCH. Statistical differences between the CWC values of each grove were calculated using one way ANOVA and post-hoc Tukey test to determine statistical differences between groves for both years and for the change between years.

2.5. Environmental correlates

To gain an understanding of the environmental correlates of

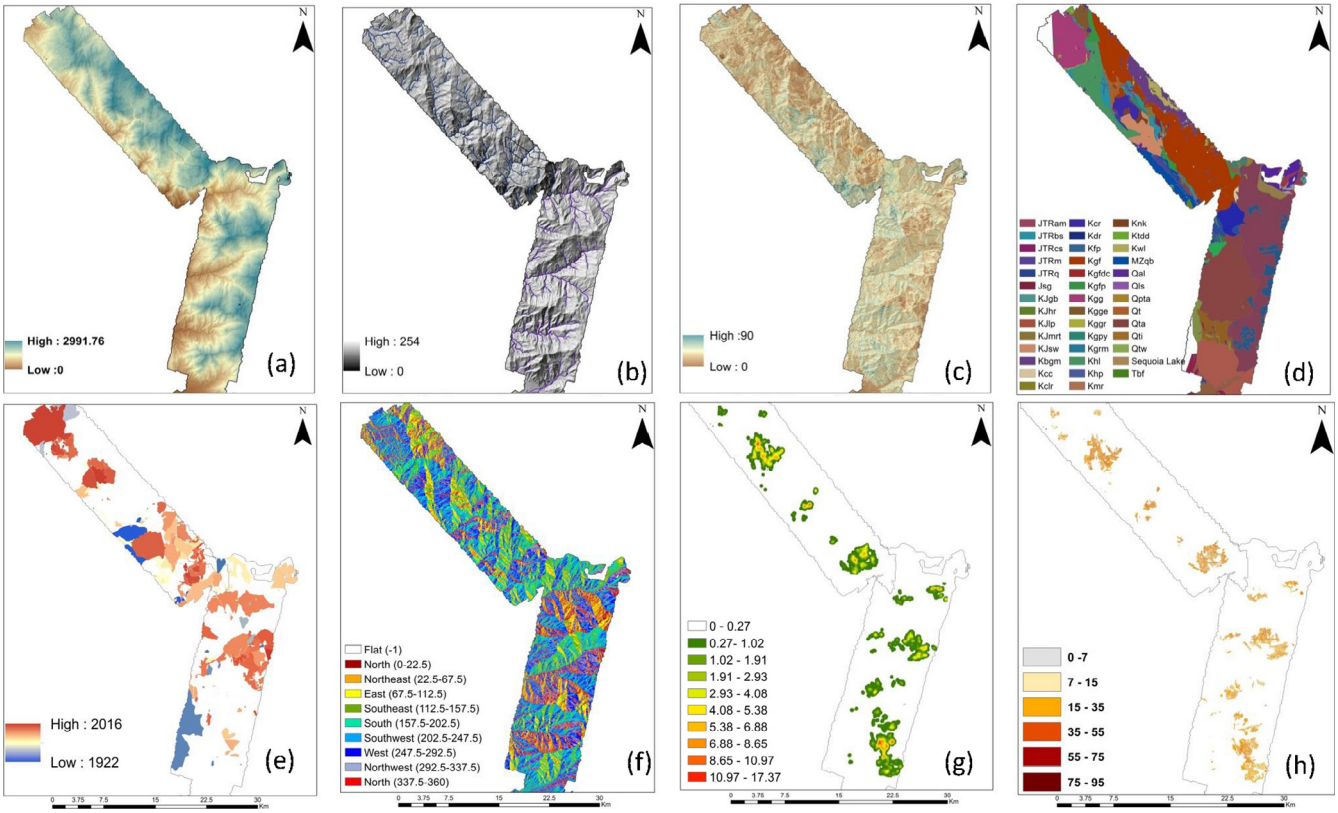

Fig. 4. Subset of geospatial datasets used in the Random Forest Machine Learning (RFML) algorithm to study the environmental correlates on canopy water content change along a giant sequoia grove elevation gradient: (a) elevation above sea level (m), (b) hillshade and rivers and streams (m), (c) slope (degrees), (d) geology (class) (e) fire history (year of last fire; 1922–2016) (f) aspect (degrees), (g) sequoia density (points within a 100 meter radius) and (h) top canopy height in sequoia groves (m).

2015–2016 CWC change in giant sequoias at a landscape scale, we investigated 15 environmental variables categorized into six groups: topography, geology, hydrology, climate, forest structure, and disturbances (examples shown in Fig. 4). We investigated the influence of these environmental correlates on CWC using a Random Forest Machine Learning (RFML) algorithm. RFML utilizes multiple decision trees to estimate the interactions between the input data (the environmental correlates) and the response variable (CWC change) using a random subset of the input variables during the construction of each tree (Breiman, 2001).

The topographic variables were derived from the LiDAR DEM, and included slope, aspect, hillshade, and elevation (Table 2). A hydrological variable, distance from streams, was calculated using the Euclidean distance from perennial creek with up to 500 m distance from streams as maximum distance from water. DEM-based models were created with the Geomorphometric and Gradient Metrics Toolbox (Evans et al., 2011) and the Arc-Hydro Toolbox (Maidment, 2002) and implemented with ESRI ArcGIS software (ESRI ArcMap 10.2.2 Redlands, California, USA). Climatic variables included climatic water deficit (CWD), runoff, and soil water storage (STOR), which were all derived from average historical data (1981–2010) using a basin characterization model (BCM) (Flint et al., 2013). The BCM is a regional climate model using a monthly time step to simulate hydrologic responses to climate at a spatial resolution of 250 m. Additionally, we calculated the compound topographic index (CTI), also known as the topographic wetness index (TWI), which is a function of the slope and

Table 2
The environmental variables considered for analysis in association with giant sequoia canopy water content change; bold type indicates variables that were not included in the model.

Categories	Factors	Units	Spatial scale	Model
Topography	Elevation	m	2 m	LiDAR data-DEM in 2-m resolution
	Slope	°	2 m	
	Hillshade	°	2 m	
	Aspect	°	2 m	
Hydrology	Distance from river or stream	m	2 m	Arc-Hydro model and Euclidean distance
Substrate	Geology	Class		USGS-GIS dataset
Climate	Climatic water deficit (CWD)	mm	250 m	Basin Characterization Model (BCM)
	Soil water storage	**mm**	**250 m**	
	Runoff	**mm**	**250 m**	
	Compound topographic index (CTI)			
Forest structure	Sequoia density	100 m radius	3.14 ha	
	Top canopy height	m	2 m	LiDAR data
Disturbances	**Fire frequency**	**Frequency; number since 1922**		**SEKI historical fire data from 1922 to 2015**
	Time since last fire	TSLF; since 1922		SEKI historical fire data from 1922 to 2015

the upstream contribution area (Moore et al., 1993). The substrate variable included geology, derived from a geological geo-database supplied by the National Park Service Geologic Resources Inventory program, and contains 23 different geological classes.

The forest structure variables included giant sequoia density, calculated as the density of central points in the crown or clump of sequoia crowns within a 100 m radius, and tree height, derived from the LiDAR data for each identified giant sequoia crown or clump of crowns. Finally, two disturbance variables were used, both of which were constructed from fire history data from 1922 until 2016 (Caprio and Lineback, 2002). These two derived variables were average fire frequency (FF) and time since last fire (TSLF), following Asner et al. (2016b).

Using the RFML model, we estimated the relative importance of the predictor variables to CWC change. Relative importance is represented by the influence of the different prediction variables on giant sequoia CWC change. We then characterized how different predictor variables in isolation (or in pairs) influenced CWC change using partial dependence plots (PDPs). In these PDPs, only the predictor variable(s) of interest were allowed to vary, and the rest remain constant; the response (CWC change) is then averaged over all other instances of the data for each value of the predictor variable(s) (Friedman, 2001). To estimate model performance, we used the regression coefficient and root mean square error (RMSE) on a 10-fold cross validation. All of the analyses were conducted in the machine learning platform H2O with a Python interface (Baldominos et al., 2014). Each of these environmental variables was scaled up or down to match the 2 m resolution grid, such that cells from all maps were geospatially aligned. Collinearity between predictor variables was assessed prior to analysis using Spearman rank correlation tests (Zuur et al., 2010). TSLF was found to be correlated with FF, and soil water storage (SWT) and runoff were found to be correlated with climatic water deficit (CWD) ($R \geq 0.65$). Therefore STOR, runoff, and FF were discarded from all analyses (Appendix A).

3. Results

3.1. Mapping of giant sequoias

We applied the GBM model to the HiFIS image, which resulted in a pixel classification as 'sequoia' or 'other trees' for each pixel across the landscape. The classification accuracy of giant sequoia pixels in the north and south areas were both high, at 95% and 98%, respectively. The pixel-level cross-validation of the final models is shown in Table 3, referring to the northern and southern areas of the 2015 imagery. The resulting spatial pattern of giant sequoia distribution agreed with our knowledge of sequoia groves in the southern Sierra Nevada range (Fig. 1). Fig. 5 shows the giant sequoia crowns and clumps of crowns identified in Redwood Mountain grove and their CWC values as an example of the mapping output. We used each grove area as delineated by national park managers to estimate the number of giant sequoia crowns or clumps of crowns within each grove or aggregation of groves (Table 4). The aggregation of groves was based on a minimum number of 5 crowns or clump of crowns that will be suitable for statistical analysis. We estimate a total of 14,225 giant sequoia crowns and clumps of crowns in the northern and southern area for a combined grove area of 5782.51 ha. The estimated giant sequoia crowns or clumps shown in Table 4 are not intended to be an absolute count of sequoias, due to our shade filtering that removes smaller and shaded crowns from the analyses.

Table 3
Confusion matrix for the gradient boosting machine (GBM) classification model resulting in two classes of pixels, "giant sequoia" and "other trees," for the calibration and validation sets. The confusion matrix reports the number of *false positives*, *false negatives*, *true positives*, and *true negatives* classifications of "giant sequoias" and "other trees".

South 2015 calibration	Other trees	Giant sequoias		Overall accuracy
Other trees	3851	10	3861	
Giant sequoias	15	1380	1395	
Total	3866	1390	5256	
Accuracy	0.996	0.993		0.995
Validation	Other trees	Giant sequoias		
Other trees	416	4	420	
Giant sequoias	5	140	145	
Total	421	144	565	
Accuracy	0.99	0.97		0.98
North 2015 calibration	Other trees	Giant sequoias		
Other trees	2594	19	2613	
Giant sequoias	25	1342	1367	
Total	2619	1361	3980	
Accuracy	0.97	0.99		0.98
Validation	Other trees	Giant sequoias		
Other trees	300	13	313	
Giant sequoias	8	160	168	
Total	308	173	481	
Accuracy	0.974	0.925		0.952

3.2. Canopy water content and change

The CWC values from August 2015 and July 2016 were both collected during the dry seasons. These values are also a reflection of the effects of progressive drought from 2012 to 2016. Within the drought years, 2014 was identified as the single most extreme summer drought in the 122-year record (Stephenson et al., this issue). Giant sequoia CWC ranged from 1.6 to 7 L m^{-2} (for crowns or clump of crowns), was extremely variable in a spatial context within and between the study groves, and displayed a patchy pattern in both years (Fig. 6). The highest CWC values in 2015 and 2016 were found in the groves with high sequoia densities (Fig. 6). Fig. 7 provides box-whisker plots of the mean CWC variation and the proportional CWC change in 33 groves or aggregated groves that were mapped in 2015 and 2016. Mean CWC values increased from 2015 to 2016 from 3.97 to 4.19 L m^{-2}, indicating a general trend of recovery, which aligns with the Stephenson et al. (this issue) findings of no substantial additional foliage dieback following 2014 (Fig. 7c). Additionally, variation in CWC was greater in 2016 than in 2015 (Fig. 7c). Significant inter-grove differences were found in the proportional CWC change with high CWC loss in the groves: Sequoia Creek, Big Stump, Pine Ridge, Skagway, Oriole Lake, Coffeepot Canyon and Surprise groves ($p \geq 0.05$, $F_{(31;\ 13971)} = 116.06$ $p \leq 0.05$). In addition, the Redwood Mountain Grove showed a reduction in mean CWC from 2015 to 2016 (Fig. 7). We found significant increases (gain) in CWC in Redwood Meadow, Little Redwood Meadow, Granite Creek and East Fork groves. We found a positive but weak correlation between grove size and CWC change ($R = 0.15$). Canopy water content declined in eight of the eleven smallest groves (0.33–18.97 ha), five of the eleven intermediate groves (21.37–93.8 ha), and in only one of the eleven largest groves (99.78–1038.36 ha). Fig. 8 shows the result of the proportional CWC change for the north and south areas. Correlations between CWC of giant sequoias in the northern and southern areas in 2015 and 2016 are shown in Appendix B.

3.3. Environmental correlates

The RFML model indicated that a hierarchy of environmental correlates is related to the variation in giant sequoia CWC change at a landscape scale (Fig. 9). The RFML model included a regression coefficient (R^2) = 0.54 for the CWC change model. Analysis of the CWC change against the environmental correlates identified geology and elevation as the most important factors related to CWC change throughout the network of sequoia groves (Fig. 9), accounting for a combined 38.05% of the CWC change that was explained by the model.

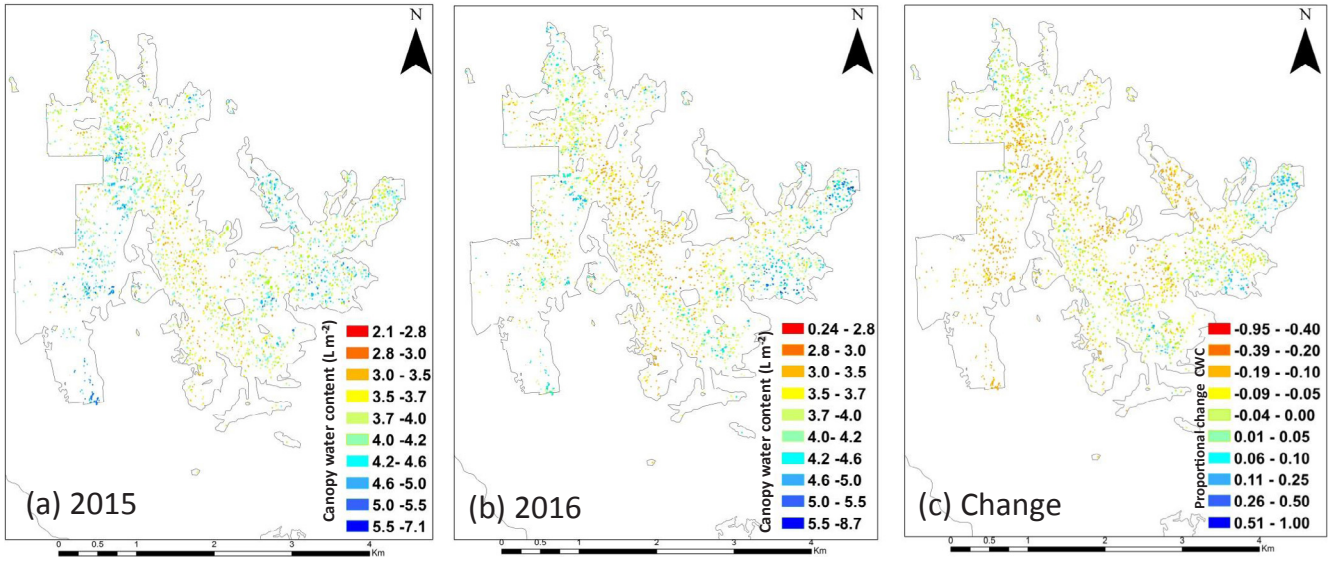

Fig. 5. Canopy water content (CWC) of giant sequoia crowns in the Redwood Mountain grove from 2015 (a), 2016 (b), and the proportional change (c). The CWC units are liters of water per square meter (L m^{-2}). The white color refers to areas where no sequoia crowns were detected by our approach, although they may still have been present.

Table 4
Summary of the grove numbers and names with the estimated area of giant sequoia crowns or clumps of crowns numbers that were mapped in Sequoia Kings Canyon National Park and vicinity. The estimated number of giant sequoia crowns or clumps is not intended to be an absolute count of sequoias, due to our shade filtering that removes smaller and shaded crowns from the analyses.

Grove No.	Grove Name	Estimated area (ha)	Estimated number of giant sequoia crowns or clumps
1	Bearskin Grove	64.96	75
2	General Grant	84.86	116
3	Sequoia Creek	14.06	5
4	Big Stump & Big Baldy South	100.37	5
5	Redwood Mountain	1038.36	3269
6	Lost	21.37	92
7	Muir	154.14	452
8	Pine Ridge	28.64	44
9	Skagway	35.32	29
10	Suwanee	42.11	108
11	Giant Forest	935.48	2429
12	Granite Creek	1.28	6
13	Redwood Meadow	146.81	564
14	Castle Creek	169.54	236
15	Little Redwood Meadow	18.98	92
16	Atwell	541.68	846
17	Oriole Lake &Douglass & Squirrel Creek	99.78	233
18	Redwood Creek	41.8	57
19	East Fork	397.44	1062
20	New Oriole Lake	15.24	34
21	Eden Creek	290.38	463
22	Horse Creek	43.96	90
23	Cahoon &Lower Horse Creek	16.11	21
24	Coffeepot Canyon	9.68	11
25	Surprise	15.14	12
26	Homers Nose	93.8	143
27	Board Camp	40.35	48
28	Cedar Flat	13.17	52
29	South Fork	166.69	327
30	Garfield	623.63	2121
31	Devil's Canyon & Forgotten	6.44	14
32	Dennison	8.58	18
33	Dillonwood	502.36	1151
		5782.51	14225

The next two most important factors were climatic water deficit (CWD) and distance from streams, which accounted for a combined additional 20.3%. Several other minor factors also contributed to the mapped variation in CWC change, including giant sequoia density (7.4%), and TCH (7.14%). The remaining five factors (slope, aspect, hillshade, CTI, and TSLF) had much less influence on CWC change accounting for a combined additional 27.05% relative influence on CWC change (Fig. 9).

Partial dependence plots (PDPs) derived from the RFML models were used to explore how different environmental variables influence spatial variation in CWC change in giant sequoias. Because all predictor variables other than the one or two being examined are held constant, PDPs show the average response of CWC change over the entire range of predictor variables as a function of the variable being examined, and consequently do not highlight the specific nonlinear interactions between the prediction variables. CWC change in giant sequoias showed losses in the geological areas of granodiorite of Milk Ranch Peak (Kgmr), Mesozoic (MZcs), mafic met volcanic rocks (Mzmm), and showed gains in Tioga and Tahoe Tills (Qtw), granodiorite of Castle Creek (Kcc) and in coarse porphyritic facies (Kmpc) (Sisson and Moore, 1994). In addition, the PDPs indicated CWC losses at lower elevations and CWC gains in the high elevations (Fig. 10). Higher climatic water deficit values indicated declines in CWC. The PDPs showed that giant sequoias adjacent to streams had greater gains in CWC, and showed CWC losses increasing with the distance from water sources (Fig. 10a). In addition, we found that areas with high sequoia densities had high CWC gains, and in areas where the sequoia density decreases, there was a higher CWC loss. We also found that shorter sequoia trees had a greater CWC loss, with greater loss in trees that were shorter than 40 m. Terrain played a role in mediating CWC loss in giant sequoias, with greater CWC losses found on steeper slopes than on shallow terrain. In addition, greater CWC losses were found on the northeast-facing slopes (Appendix C).

4. Discussion

We estimated giant sequoia response to drought stress using remotely sensed CWC as an indicator for canopy-level foliage status. Giant sequoia crowns were mapped with high accuracy, and their CWC values in both 2015 and 2016 were measured. Our results suggest that giant sequoia response to droughts is spatially variable, and that at least some of that variability can be explained by the geological substrate, elevation and site-specific water balance. Water balance describes

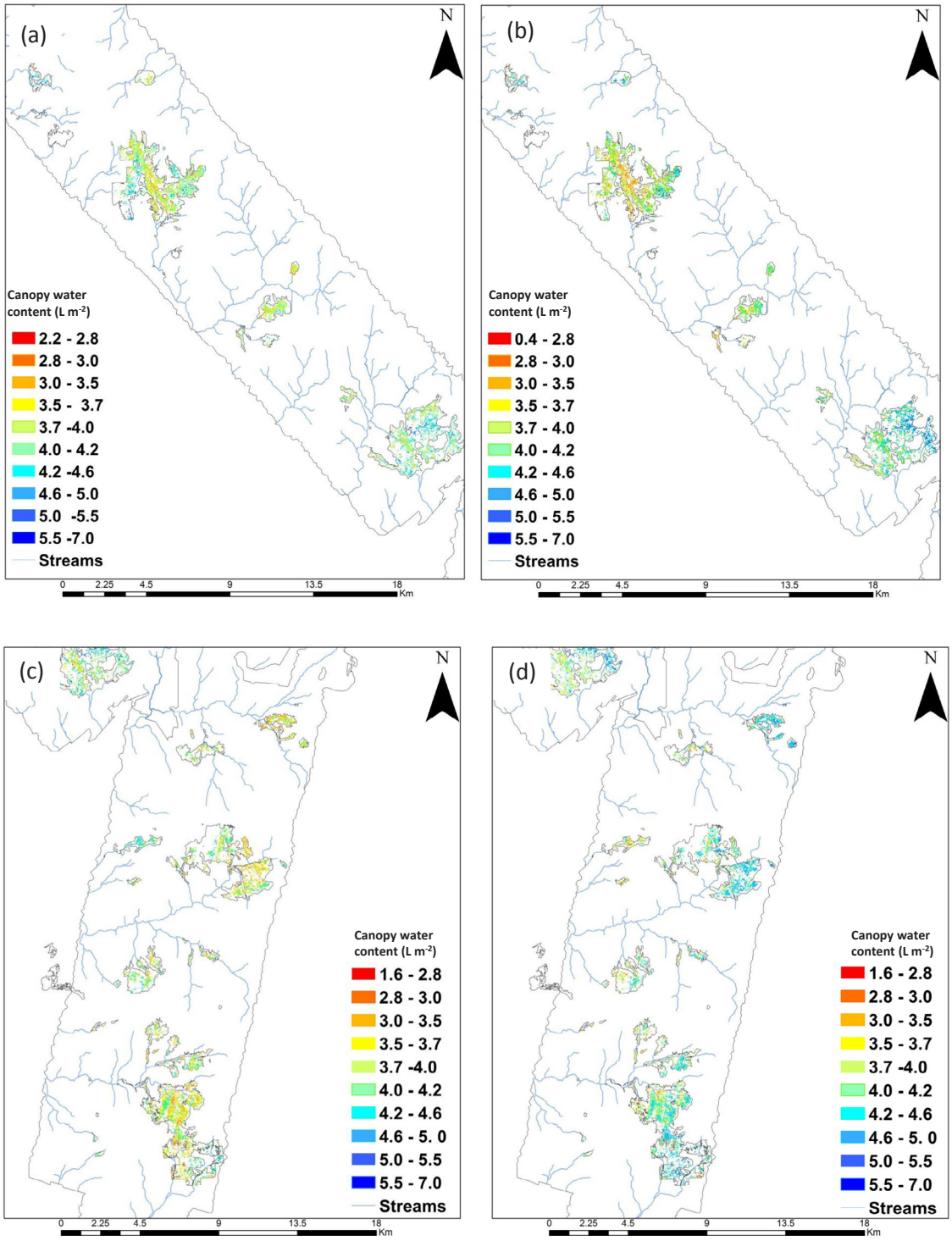

Fig. 6. Distribution of mapped canopy water content (CWC) for giant sequoias for the years (a) 2015 north, (b) 2016 north, (c) 2015 south, and (d) 2016 south throughout the study area. The CWC units are in liters of water per square meter (L m^{-2}).

climate as it is sensed by plants and is related to the interaction of energy, water and the environment (Stephenson, 1988; Stephenson, 1990). We found the spatial variation in CWC is associated with metrics of water availability known to be influenced by the site water balance and site-specific conditions (e.g., topography). We found that greater CWC loss is related to specific geological substrate and to lower elevations in areas with high climatic water deficit (CWD) values, in areas with greater distances from water sources, and on steeper slopes. In addition, we found that shorter giant sequoias and those growing in lower sequoia density have greater CWC loss. The environmental correlates indicate that site specific conditions mediate CWC gains or losses and may indicate site suitability. We suggest using changes in giant sequoia CWC as a long-term metric for understanding their response to climate variability and change, which is essential to capture the spatial patterns and variation in CWC change in response to drought stress.

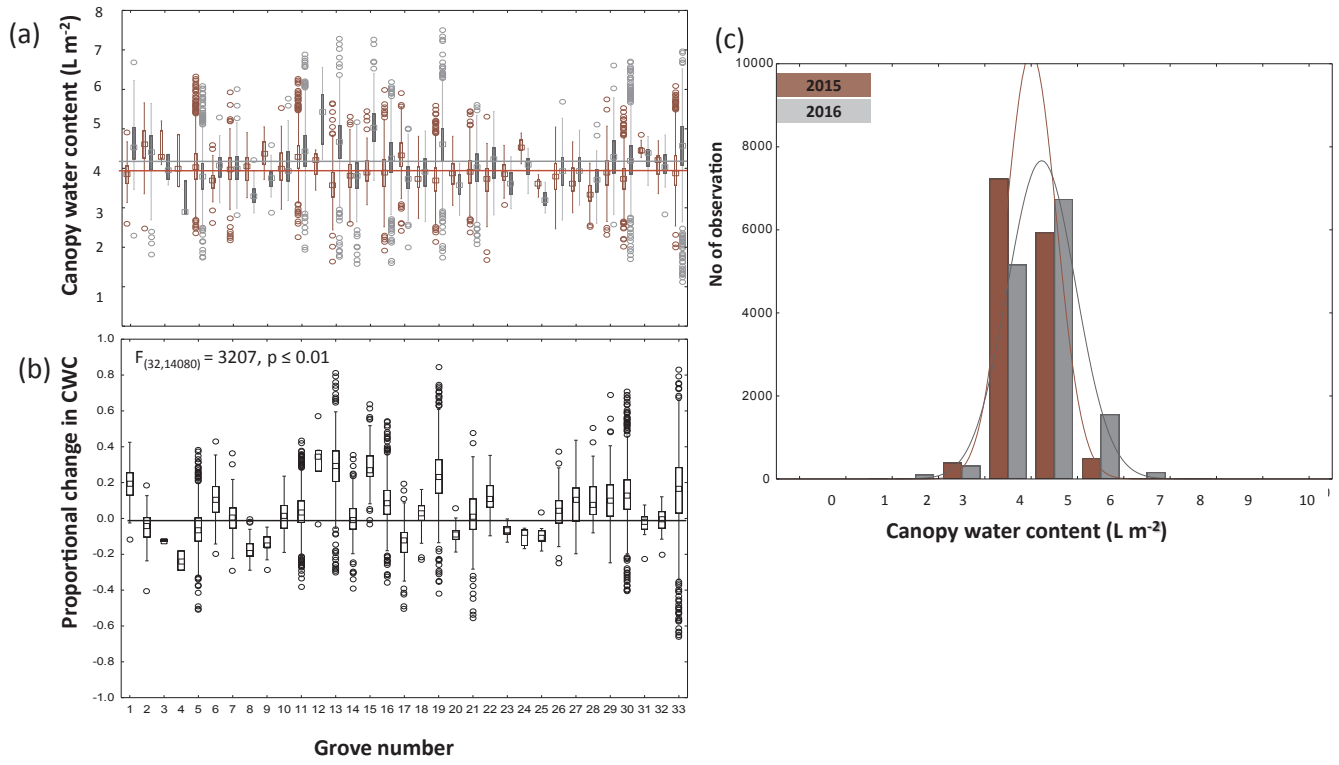

Fig. 7. (a) Box-whisker plots showing mean crown variation in canopy water content (CWC) in giant sequoia groves for 2015 and 2016 and (b) box-whisker plots showing regional variation in proportional CWC change at the giant sequoia crown-level, (c) histogram of CWC in giant sequoia groves for 2015 and for 2016. Grove numbers correspond to those in Table 4.

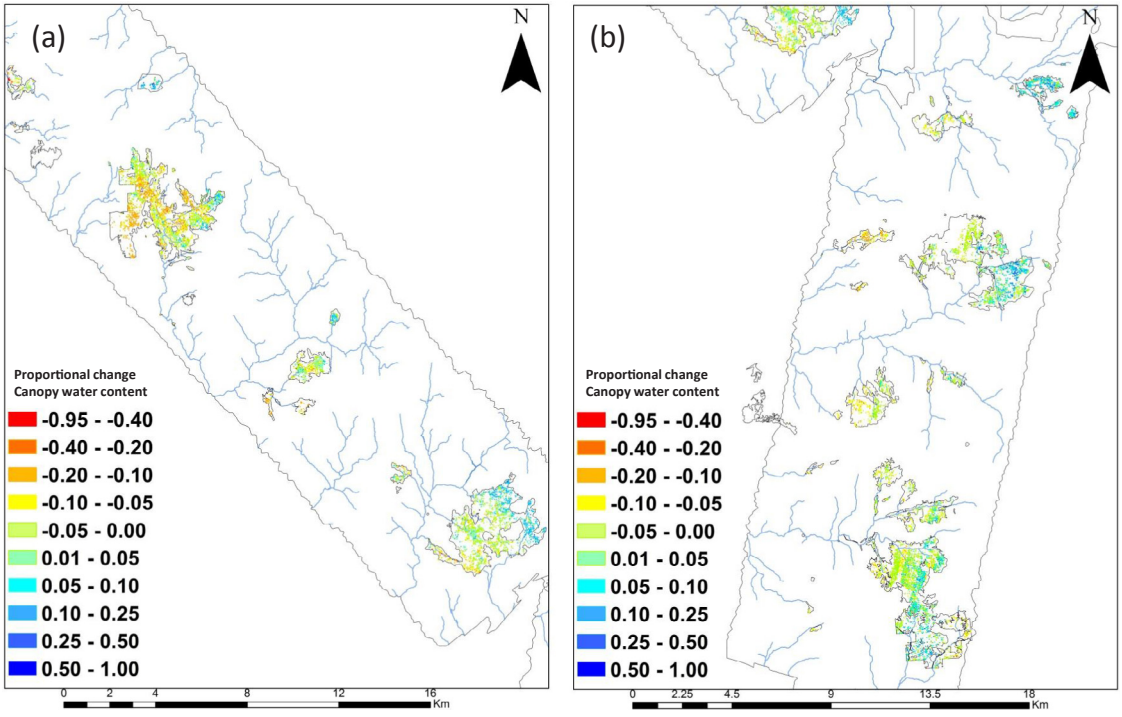

Fig. 8. Distribution of mapped giant sequoia proportional canopy water content (CWC) change from 2015 to 2016 for the north (a) and south area (b).

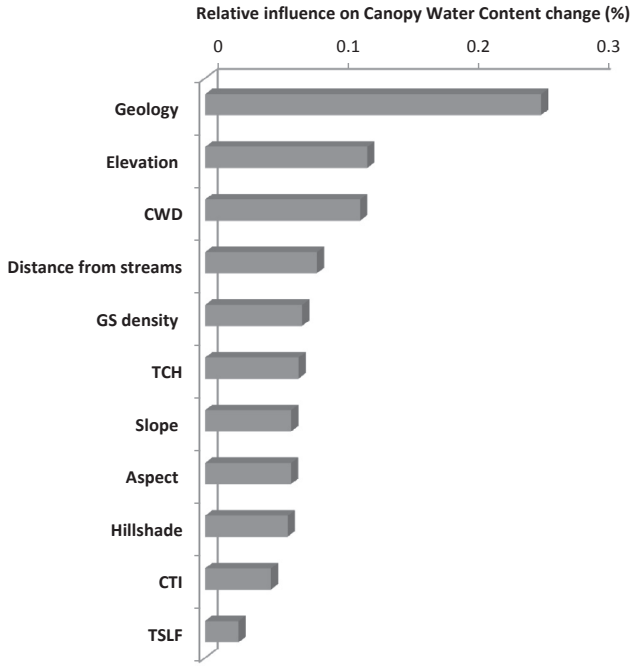

Fig. 9. Relative influence of environmental correlates on giant sequoia canopy water content (CWC) change.

4.1. Canopy water content variation in space and time

Tree responses to drought vary at multiple scales, from cells to population levels. Ambrose et al. (this issue) described several leaf-level responses in giant sequoia. Martin et al. (this issue) established a relationship between CWC and foliage dieback, suggesting that CWC, and changes in CWC, may be powerful indicators of stress in giant sequoias. We quantified CWC change as an indicator of giant sequoia population-level responses to drought across a series of groves. The CWC values displayed a patchy pattern with high variability within grove and among the groves at the landscape scale (giant sequoia CWC ranged from 1.6 to 7 $L\,m^{-2}$). CWC change through time may thus provide a basis for identifying giant sequoia crowns that are more or less susceptible or resilient to drought stress. The integration of HiFIS and LiDAR measurements with ground-based assessments of environmental and ecological changes will help identify where giant sequoias are most at risk. A multidisciplinary approach, combining remotely sensed CWC observations with targeted ground-based monitoring of the local susceptibility or resilience of crowns, is likely required. Once at-risk regions and trees have been identified, management can be adapted to reduce the risks in prioritized populations, and promote long-term adaptation to climatic change (see Nydick et al., 2017).

4.2. Environmental correlates

Environmental correlates such as topography, climate, hydrology, geology and soil substrates are known to influence the forest water balance in mountainous terrain, causing a spatial pattern in water availability (e.g. Guarín and Taylor, 2005; Lang et al., 2013; Anning et al., 2014), which likely affects CWC. Soil moisture and water balance are known to have critical ecological significance in giant sequoias (Rundel, 1972). We found that geological substrate and elevation had the greatest relative importance in explaining variation in CWC change among sequoia groves. However, interpretation of this apparent role of geological substrate will require further work to distinguish between two possibilities. First, the geological substrate classifications were finely divided spatially, meaning that most groves were located on substrate classifications that were distinct from one another. This leaves open the possibility that geological substrates are incidentally correlated with other factors – factors not directly related to the finely-divided classifications – that could affect CWC change, such availability of belowground water from outside grove boundaries. Second, CWC change might indeed be influenced by the effects of geological substrate on soil water-holding capacity and/or soil chemistry (cf. Hahm et al., 2014). Distinguishing between these possibilities will require direct measurements of biologically-meaningful soil and substrate properties, which are currently unavailable to us.

We found that lower elevations experienced greater CWC losses, where evaporative demand is greater and snowpack duration is reduced (Fig. 10). These results complement other studies indicating elevated tree mortality from low- to mid-elevation coniferous tree species in the Sierra Nevada during the 2012–2016 droughts (Asner et al., 2016a, 2016b; Paz-Kagan et al., 2017). The same pattern of elevated foliage

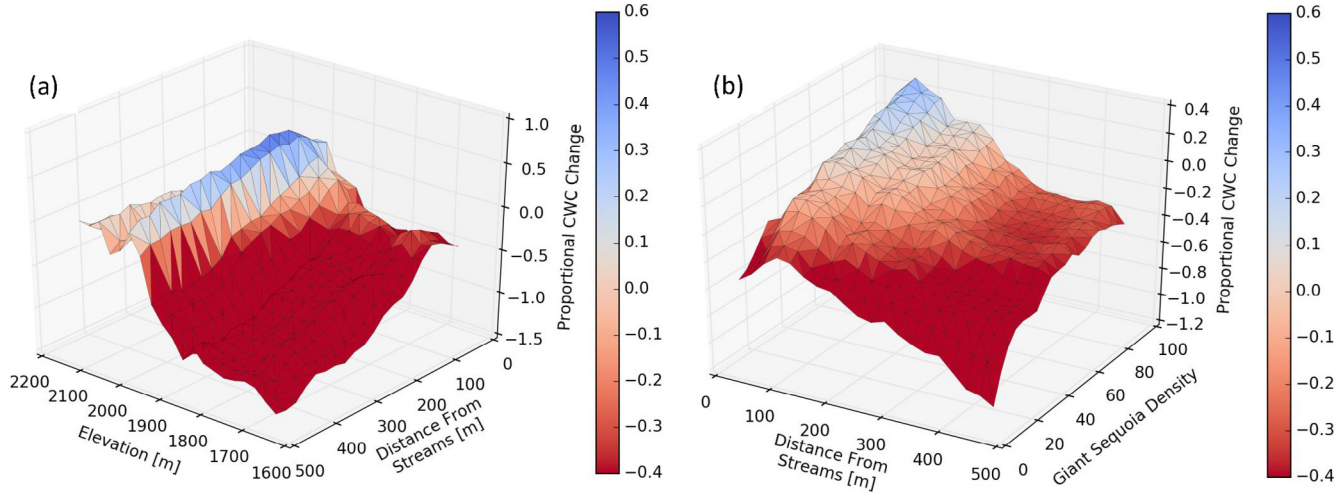

Fig. 10. Partial dependency plots (PDPs) displaying the predicted proportional average giant sequoia canopy water content (CWC) change for: (a) elevation above sea level (m) and distance from streams (m) and (b) distance from streams (m) and giant sequoia density (points in a 100 m radius).

dieback in giant sequoias was identified by Stephenson et al. (this issue).

Climatic water deficit, and distance from streams, which were the next most important factors correlated with CWC change, are also related to water availability and soil moisture at the landscape level (Anderegg et al., 2013). Giant sequoias located at the margins of creeks are supported by high water availability (Ambrose et al., 2016). We found increased CWC loss with farther distances (more than 200 m) from streams. We also found that steeper slopes harbored greater CWC loss, likely because water is more prone to runoff. Other research has found that, for sequoia groves in general, low-elevation groves consistently appear either along a stream or low on a slope with steady groundwater drainage (Rundel, 1972). Across the entire natural range of giant sequoias, groves also demonstrate different preferences for aspect, for example the northern disjunctive groves largely exist at elevations ranging between 1400 and 2000 m, favoring the south-facing slopes. However, the major group of groves south of the Kings River generally exist at higher elevations, up to 2450 m, with individual trees growing at an elevation up to 2700 m, and favoring the north-facing slopes (Fites-Kaufman et al., 2007). These environmental mediators are related to places with CWC loss or gain and reflect site suitability in general, which is then amplified during drought.

The correlation between the forest structural variables (tree density and height) and CWC change may be rooted in biological explanations such as tree physiology. Other studies suggest that trees response to drought stress is size-dependent and diverse among tree species and that both short and tall trees may be more vulnerable to drought than intermediate size trees (Das et al., 2007; Colangelo et al., 2017). The greater sensitivity of taller trees may be associated with hydraulic constraints that increase with tree height, as a consequence of both increasing hydraulic path length with greater height and higher evaporative demands in the upper canopy (Lang et al., 2013; McDowell and Allen, 2015). The greater sensitivity of shorter trees may be related to competition or less developed root systems attempting to gain access to groundwater (Hember et al., 2016). We found that the shorter sequoia trees have a greater CWC loss and that the taller trees appear to have small CWC changes. However, these results could merit more detailed examination in future studies by exploring the hydraulic constraints with response to the height of sequoia trees. In addition, we found that giant sequoia density was negatively related to CWC loss, perhaps because wetter parts of groves – in addition to being more buffered from drought – are more favorable to high densities of sequoias (Fig. 10). These results suggest that trees on the edges of groves, growing in marginal habitats, may be the first responders to drying conditions. We suggest that additional aspects need to be taken into consideration, for example, a high density area might host bigger sequoias with deeper roots. This can also be associated with grove size, since small groves will have a greater proportion of sequoias located along grove edges in comparison to sequoias in large groves that are dominated by interior effects. These responses are a combination of phenological and physiological responses that may add insights to environmental metrics used in this study. For example, canopy distance from grove boundary might be used in future analysis as a variable to explain vulnerability and targeting treatments.

4.3. Landscape-scale approach for management of giant sequoia groves

Drought is one of the primary environmental factors limiting the growth, distribution and survival of trees species worldwide (e.g.Allen and Breshears, 1998). As droughts become hotter and more frequent, with greater severity and longer duration in many regions of the world, forest vulnerability increases, evidenced by widespread tree mortality and CWC loss (Allen et al., 2015; Asner et al., 2016a). Our results reveal that giant sequoias response to future droughts is likely to be spatially quite variable, and that at least some of that variability can be explained by site water availability and site specific conditions. The extent to which tree species can tolerate water-stress conditions also depends upon phenotypic variation, strength of selection, fecundity, inter-specific competition, and biotic interactions (Aitken et al., 2008).

The giant sequoias are a classic example of paleoendemic taxa whose origins predate the Mediterranean ecosystem that they currently occupy. Giant sequoias have lived for thousands of years, and not surprisingly, they are located in an area with a relatively abundant water supply. Dodd and DeSilva (2016) provide evidence that climatic events during the last 2 million years had important consequences for the current distribution of giant sequoias' genetic diversity. Giant sequoias have a fragmented distribution associated with increasing aridity, and their numbers apparently declined during the early and middle Holocene (Anderson and Smith, 1994). Future warming may decrease the amount of soil moisture, water availability, and snowpack (Belmecheri et al., 2016), making the conditions throughout the Sierra Nevada unfavorable for giant sequoias due to their low genetic diversity, limited distribution (Dodd and DeSilva, 2016), and high water demand (Ambrose et al., 2016). Sequoia and Kings Canyon national parks warmed by about 0.58 °C between 1975 and 2011 (Das and Stephenson, 2013) and by the end of the century, another 1.1–2 °C of warming in the winter and 2.2–4.4 °C in the summer is expected in the Sierra Nevada (Safford et al., 2012). These trends may increase evaporative demand, which in large trees may have a greater impact due to their large leaf areas and their high water demands (Bennett et al., 2015; McDowell and Allen, 2015).

5. Conclusions

Our results suggest that HiFIS and LiDAR imagery can be used to map giant sequoia distribution throughout the southern Sierra Nevada in central California. Using these airborne measurements, we were able to classify giant sequoias with high accuracy. We used CWC and CWC change as indicators of giant sequoias' foliage status, which enabled us to assess a critical component of giant sequoias' response to drought stress. We also analyzed environmental correlates of CWC change (recovery or losses), and found that geology, topography, and hydrology were key correlates. In addition, our findings suggest that shorter sequoia trees and those growing in areas with lower sequoia density have a greater CWC loss. Future warming may decrease the amount of soil moisture, making the conditions throughout the Sierra Nevada unfavorable for giant sequoias. Therefore, long-term monitoring of the CWC of giant sequoias can inform and support decision-making and forest management practices to help prepare for future droughts.

Acknowledgements

We thank C. Anderson and D. Knapp for assistance with airborne data collection and processing. For feedback, ideas, and suggestions, we thank our collaborators in the Leaf to Landscape forest drought project, particularly A. Ambrose, W. Baxter, T. Dawson, and E. Francis. This study was funded by the David and Lucile Packard Foundation, the U.S. National Park Service and the U.S. Geological Survey's Ecosystems and Climate and Land Use Research and Development programs and the USGS Southwest Climate Science Center. The Carnegie Airborne Observatory has been made possible by grants and donations to G.P. Asner from the Avatar Alliance Foundation, the Margaret A. Cargill Foundation, the David and Lucile Packard Foundation, the Gordon and Betty Moore Foundation, the Grantham Foundation for the Protection of the Environment, the W. M. Keck Foundation, the John D. and Catherine T. MacArthur Foundation, the Andrew Mellon Foundation, Mary Anne Nyburg Baker and G. Leonard Baker Jr, and William R. Hearst III. Any use of trade, firm, or product names is for descriptive purposes only and does not imply endorsement by the U.S. Government.

Appendix A

Spearman rank correlation tests for the environmental factors in Sequoia and Kings Canyon National Parks (SEKI) and vicinity. Bold numbers indicate significant differences with $R \geq 0.5$. The full names of the environmental factors are given in Table 2.

Variables	Geology	Runoff	SWT	CWD	GS density	D. streams	CTI	Elevation	Hillshade	TCH	Slope	Aspect	FF	TSLF
Geology	**	−0.165	0.169	0.068	−0.241	0.017	−0.029	−0.229	−0.172	0.051	0.117	−0.089	−0.182	−0.277
Runoff	−0.165	**	**−0.86**	0.272	0.223	−0.131	0.008	0.363	0.269	0.153	0.058	0.148	0.116	0.227
STW	0.169	**−0.86**	**	−0.639	−0.237	0.08	0.009	−0.169	−0.328	−0.077	−0.11	−0.136	0.151	0.002
CWD	0.068	0.272	−0.639	**	−0.006	0.226	−0.013	−0.482	0.168	−0.086	0.067	0.004	−0.397	−0.291
GS. density	−0.241	0.223	−0.237	−0.006	**	−0.199	0.044	0.213	0.073	0.191	−0.128	0.032	−0.062	−0.023
D. streams	0.017	−0.131	0.08	0.226	−0.199	**	0.003	−0.454	−0.016	−0.104	−0.05	−0.042	−0.002	−0.017
CTI	−0.029	0.008	0.009	−0.013	0.044	0.003	**	−0.054	0.062	−0.015	−0.311	0.038	0.022	0.037
Elevation	−0.229	0.363	−0.169	−0.482	0.213	−0.454	−0.054	**	−0.058	0.135	0.148	0.022	0.309	0.274
Hillshade	−0.172	0.269	−0.328	0.168	0.073	−0.016	0.062	−0.058	**	0.005	−0.113	0.64	−0.175	0.032
TCH	0.051	0.153	−0.077	−0.086	0.191	−0.104	−0.015	0.135	0.005	**	−0.05	−0.035	0.09	0.037
Slope	0.117	0.058	−0.11	0.067	−0.128	−0.05	−0.311	0.148	−0.113	−0.05	**	−0.041	0.046	0.004
Aspect	−0.089	0.148	−0.136	0.004	0.032	−0.042	0.038	0.022	0.64	−0.035	−0.041	**	−0.063	0.056
FF	−0.182	0.116	0.151	−0.397	−0.062	−0.002	0.022	0.309	−0.175	0.09	0.046	−0.063	**	**0.899**
TSLF	−0.277	0.227	0.002	−0.291	−0.023	−0.017	0.037	0.274	0.032	0.037	0.004	0.056	**0.899**	**

Appendix B

Correlations among canopy water content (CWC) of crowns and clumps of crowns of giant sequoia in the northern (a) and southern (b) and combined model for 2015 and 2016.

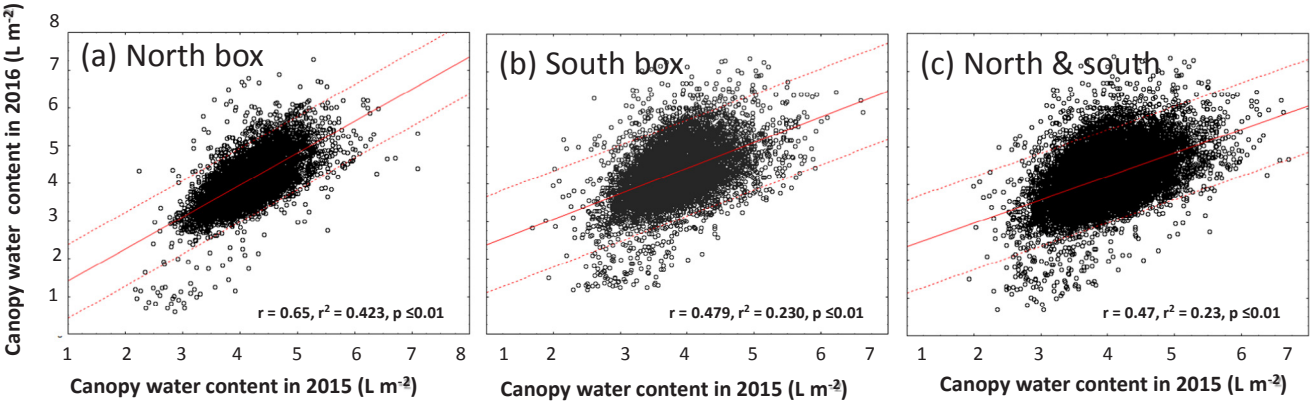
(a) North box
(b) South box
(c) North & south
Canopy water content in 2016 (L m-2)
Canopy water content in 2015 (L m-2)
r = 0.65, r2 = 0.423, p ≤0.01
r = 0.479, r2 = 0.230, p ≤0.01
r = 0.47, r2 = 0.23, p ≤0.01

Appendix C

Partial dependence plot (PDPs) displays the change in the canopy water content of giant sequoias over the range of one predictor factor. (a) Elevation above sea level (m); (b) Distance from streams (m); (c) Topographic aspect (degrees); (d) Slope steepness (degrees);(e) climatic water deficit (CWD) (mm/year); (f) compound topographic index (CTI); (g) Giant sequoia density; (h) Top canopy height (tree size, m); (i) Hillshade (j) Geology (classes); and (k) Time since last fire (TSLF; since 1922–2016).

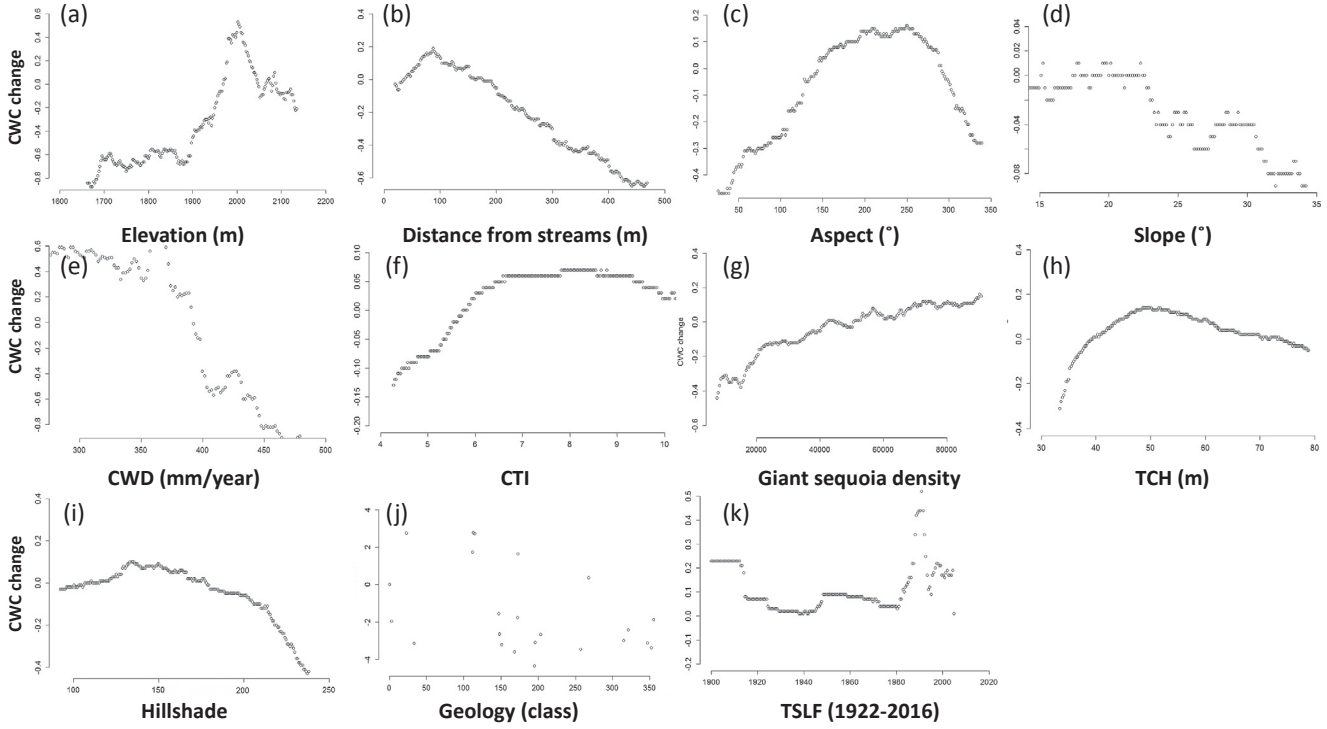

References

Aitken, S.N., Yeaman, S., Holliday, J.A., Wang, T., Curtis-McLane, S., 2008. Adaptation, migration or extirpation: climate change outcomes for tree populations. Evol. Appl. 1, 95–111.

Allen, C.D., Breshears, D.D., 1998. Drought-induced shift of a forest–woodland ecotone: rapid landscape response to climate variation. Proc. Natl. Acad. Sci. 95, 14839–14842.

Allen, C.D., Breshears, D.D., McDowell, N.G., 2015. On underestimation of global vulnerability to tree mortality and forest die-off from hotter drought in the Anthropocene. Ecosphere 6, 1–55.

Ambrose, A., Baxter, W., Martin, R., Francis, E., Nydick, K., Dawson, T., this issue. Leaf- and crown-level adjustments help giant sequoias maintain whole-tree hydraulic integrity during severe drought. For. Ecol. Manage.

Ambrose, A.R., Baxter, W.L., Wong, C.S., Burgess, S.S.O., Williams, C.B., Næsborg, R.R., Koch, G.W., Dawson, T.E., 2016. Hydraulic constraints modify optimal photosynthetic profiles in giant sequoia trees. Oecologia 182, 713–730.

Ambrose, A.R., Baxter, W.L., Wong, C.S., Næsborg, R.R., Williams, C.B., Dawson, T.E., 2015. Contrasting drought-response strategies in California redwoods. Tree Physiol. 35, 453–469.

Anderegg, W.R.L., Kane, J.M., Anderegg, L.D.L., 2013. Consequences of widespread tree mortality triggered by drought and temperature stress. Nat. Clim. Change 3, 30–36.

Anderson, R.S., Smith, S.J., 1994. Paleoclimatic interpretations of meadow sediment and pollen stratigraphies from California. Geology 22, 723–726.

Anning, A.K., Dyer, J.M., McCarthy, B.C., 2014. Tree growth response to fuel reduction treatments along a topographic moisture gradient in mixed-oak forests of Ohio, U.S.A. Can. J. For. Res. 44, 413–421.

Asner, G., Martin, R., 2015. Spectroscopic remote sensing of non-structural carbohydrates in forest canopies. Remote Sens. 7, 3526.
Asner, G.P., Anderson, C.B., Martin, R.E., Knapp, D.E., Tupayachi, R., Sinca, F., Malhi, Y., 2014. Landscape-scale changes in forest structure and functional traits along an Andes-to-Amazon elevation gradient. Biogeosciences 11, 843–856.
Asner, G.P., Brodrick, P.G., Anderson, C.B., Vaughn, N., Knapp, D.E., Martin, R.E., 2016a. Progressive forest canopy water loss during the 2012–2015 California drought. Proc. Natl. Acad. Sci. 113, E249–E255.
Asner, G.P., Knapp, D.E., Boardman, J., Green, R.O., Kennedy-Bowdoin, T., Eastwood, M., Martin, R.E., Anderson, C., Field, C.B., 2012. Carnegie airborne observatory-2: increasing science data dimensionality via high-fidelity multi-sensor fusion. Remote Sens. Environ. 124, 454–465.
Asner, G.P., Martin, R.E., Anderson, C.B., Knapp, D.E., 2015. Quantifying forest canopy traits: imaging spectroscopy versus field survey. Rem. Sens. Environ. 158, 15–27.
Asner, G.P., Nepstad, D., Cardinot, G., Ray, D., 2004. Drought stress and carbon uptake in an Amazon forest measured with spaceborne imaging spectroscopy. Proc. Natl. Acad. Sci. United States of America 101, 6039–6044.
Asner, G.P., Vaughn, N., Smit, I.P., Levick, S., 2016b. Ecosystem-scale effects of megafauna in African savannas. Ecography 39, 240–252.
Baldeck, C.A., Asner, G.P., Martin, R.E., Anderson, C.B., Knapp, D.E., Kellner, J.R., Wright, S.J., 2015. Operational tree species mapping in a diverse tropical forest with airborne imaging spectroscopy. PloS one 10, e0118403.
Baldominos, A., Albacete, E., Saez, Y., Isasi, P., 2014. A scalable machine learning online service for big data real-time analysis. In: Computational Intelligence in Big Data (CIBD), 2014 IEEE Symposium on. IEEE, pp. 1–8.
Belmecheri, S., Babst, F., Wahl, E.R., Stahle, D.W., Trouet, V., 2016. Multi-century evaluation of Sierra Nevada snowpack. Nat. Clim. Change 6, 2–3.
Bennett, A.C., McDowell, N.G., Allen, C.D., Anderson-Teixeira, K.J., 2015. Larger trees suffer most during drought in forests worldwide. Nat. Plants 1, 15139.
Breiman, L., 2001. Random forests. Mach. Learn. 45, 5–32.
Brodrick, P.G., Asner, G.P., 2017. Remotely sensed predictors of conifer tree mortality during severe drought. Environ. Res. Lett.
Caprio, A.C., Lineback, P., 2002. Pre-twentieth century fire history of Sequoia and Kings Canyon national parks: a review and evaluation of our knowledge. Assoc. Fire Ecol. Misc. Pub. 1, 180–199.
Cheng, Y.-B., Zarco-Tejada, P.J., Riaño, D., Rueda, C.A., Ustin, S.L., 2006. Estimating vegetation water content with hyperspectral data for different canopy scenarios: relationships between AVIRIS and MODIS indexes. Remote Sens. Environ. 105, 354–366.
Chin, A.R., Sillett, S.C., 2016. Phenotypic plasticity of leaves enhances water-stress tolerance and promotes hydraulic conductivity in a tall conifer. Am. J. Bot. 103, 796–807.
Clark, R.N., Swayze, G.A., Livo, K.E., Kokaly, R.F., Sutley, S.J., Dalton, J.B., McDougal, R.R., Gent, C.A., 2003. Imaging spectroscopy: Earth and planetary remote sensing with the USGS Tetracorder and expert systems. J. Geophys. Res.: Planets 108, 5131.
Colangelo, M., Camarero, J.J., Borghetti, M., Gazol, A., Gentilesca, T., Ripullone, F., 2017. Size matters a lot: drought-affected Italian oaks are smaller and show lower growth prior to tree death. Front. Plant Sci. 8.
Das, A.J., Battles, J.J., Stephenson, N.L., Van Mantgem, P.J., 2007. The relationship between tree growth patterns and likelihood of mortality: a study of two tree species in the Sierra Nevada. Can. J. Forest Res. 37, 580–597.
Das, A.J., Stephenson, N.L., 2013. A natural resource condition assessment for Sequoia and Kings Canyon National Parks: Appendix 22: climatic change. In. National Park Service.
Diffenbaugh, N.S., Swain, D.L., Touma, D., 2015. Anthropogenic warming has increased drought risk in California. Proc. Natl. Acad. Sci. 112, 3931–3936.
Dodd, R.S., DeSilva, R., 2016. Long-term demographic decline and late glacial divergence in a Californian paleoendemic: Sequoiadendron giganteum (giant sequoia). Ecol. Evolut. 6, 3342–3355.
Elith, J., Leathwick, J.R., Hastie, T., 2008. A working guide to boosted regression trees. J. Anim. Ecol. 77, 802–813.
Evans, J.S., Murphy, M.A., Holden, Z.A., Cushman, S.A., 2011. Modeling species distribution and change using random forest. In: Predictive species and habitat modeling in landscape ecology. Springer, pp. 139–159.
Farooq, M., Wahid, A., Kobayashi, N., Fujita, D., Basra, S.M.A., 2009. Plant Drought Stress: Effects, Mechanisms and Management. In: Lichtfouse, E., Navarrete, M., Debaeke, P., Véronique, S., Alberola, C. (Eds.), Sustainable Agriculture. Springer, Netherlands, Dordrecht, pp. 153–188.
Féret, J.-B., Asner, G.P., 2013. Tree species discrimination in tropical forests using airborne imaging spectroscopy. IEEE Trans. Geosci. Remote Sens. 51, 73–84.
Fites-Kaufman, J.A., Rundel, P., Stephenson, N., Weixelman, D.A., 2007. Montane and subalpine vegetation of the Sierra Nevada and Cascade ranges. Terrestrial Vegetation of California. University of California Press, Berkeley, pp. 456–501.
Flint, L.E., Flint, A.L., Thorne, J.H., Boynton, R., 2013. Fine-scale hydrologic modeling for regional landscape applications: the California Basin Characterization Model development and performance. Ecol. Process. 2, 1–21.
Friedman, J.H., 2001. Greedy function approximation: a gradient boosting machine. Ann. Stat. 1189–1232.
Friedman, J.H., Meulman, J.J., 2003. Multiple additive regression trees with application in epidemiology. Stat. Med. 22, 1365–1381.
Griffin, D., Anchukaitis, K.J., 2014. How unusual is the 2012–2014 California drought? Geophys. Res. Lett. 41, 2014GL062433.
Guarín, A., Taylor, A.H., 2005. Drought triggered tree mortality in mixed conifer forests in Yosemite National Park, California, USA. For. Ecol. Manage. 218, 229–244.
Hahm, W.J., Riebe, C.S., Lukens, C.E., Araki, S., 2014. Bedrock composition regulates mountain ecosystems and landscape evolution. Proc. Natl. Acad. Sci. 111, 3338–3343.
Hartesveldt, R.J., Harvey, H.T., Shellhammer, H.S., Stecker, R.E., 1975. The giant sequoia of the Sierra Nevada. The giant sequoia of the Sierra Nevada.
Hember, R.A., Kurz, W.A., Coops, N.C., 2016. Relationships between individual-tree mortality and water-balance variables indicate positive trends in water stress-induced tree mortality across North America. Global Change Biol.
Jump, A.S., Cavin, L., Hunter, P.D., 2010. Monitoring and managing responses to climate change at the retreating range edge of forest trees. J. Environ. Monit. 12, 1791–1798.
Jump, A.S., Mátyás, C., Peñuelas, J., 2009. The altitude-for-latitude disparity in the range retractions of woody species. Trends Ecol. Evolut. 24, 694–701.
Lang, M., McCarty, G., Oesterling, R., Yeo, I.-Y., 2013. Topographic metrics for improved mapping of forested wetlands. Wetlands 33, 141–155.
Lee, C.M., Cable, M.L., Hook, S.J., Green, R.O., Ustin, S.L., Mandl, D.J., Middleton, E.M., 2015. An introduction to the NASA Hyperspectral InfraRed Imager (HyspIRI) mission and preparatory activities. Remote Sens. Environ. 167, 6–19.
Maidment, D.R., 2002. Arc Hydro: GIS for water resources. ESRI, Inc.
Martin, E.R., Asner, P.G., Francis, E., Ambrose, A., Baxter, W., Das, J.A., Vaughn, N., Paz-Kagan, T., Dawson, T., Nydick, K., Stephenson, L.N., this issue. Remote measurement of canopy water content in giant sequoias (Sequoiadendron giganteum) during drought. For. Ecol. Manage.
McDowell, N.G., Allen, C.D., 2015. Darcy's law predicts widespread forest mortality under climate warming. Nat. Clim. Change 5, 669–672.
Meyer, M.D., Safford, H.D., 2011. Giant sequoia regeneration in groves exposed to wildfire and retention harvest. Fire Ecol. 7, 2–16.
Moore, I.D., Gessler, P.E., Nielsen, G.A., Peterson, G.A., 1993. Soil attribute prediction using terrain analysis. Soil Sci. Soc. Am. J. 57, 443–452.
Nydick, K.R., Ambrose, A., Asner, G.P., Baxter, W., Das, A.J., Martin, R.E., Paz-Kagan, T., Stephenson, N.L., 2017. The Leaf to Landscape Project: empirical mapping of climate change vulnerability for giant sequoia in the southern Sierra Nevada, CA. For. Ecol. Manage (this issue).
Omasa, K., Hosoi, F., Konishi, A., 2007. 3D lidar imaging for detecting and understanding plant responses and canopy structure. J. Exp. Bot. 58, 881–898.
Paz-Kagan, T., Brodrick, P.G., Vaughn, N.R., Das, A.J., Stephenson, N.L., Nydick, K.R., Asner, G.P., 2017. What mediates tree mortality during drought in the southern Sierra Nevada? Ecol. Appl.
Roman, D.T., Novick, K.A., Brzostek, E.R., Dragoni, D., Rahman, F., Phillips, R.P., 2015. The role of isohydric and anisohydric species in determining ecosystem-scale response to severe drought. Oecologia 179, 641–654.
Rundel, P.W., 1972. Habitat restriction in giant sequoia: the environmental control of grove boundaries. Am. Midl. Nat. 81–99.
Safford, H., North, M., Meyer, M., 2012. Climate change and the relevance of historical forest conditions.
Serbin, S.P., Singh, A., McNeil, B.E., Kingdon, C.C., Townsend, P.A., 2014. Spectroscopic determination of leaf morphological and biochemical traits for northern temperate and boreal tree species. Ecol. Appl. 24, 1651–1669.
Sisson, T.W., Moore, J.G., 1994. Geologic Map of the Giant Forest Quadrangle, Tulare County, California. US Geological Survey.
Stephenson, L.N., Dan, J.A., Ampersee, J.N., Cahill, G.K., Caprio, C.A., Sanders, E.J., Williams, A.P., this issue. Patterns and correlates of giant sequoia foliage dieback during California's 2012-2016 hotter drought. For. Ecol. Manage.
Stephenson, N., 1996. Ecology and management of giant sequoia groves.
Stephenson, N.L., 1988. Climatic Control of Vegetation Distribution: the Role of the Water Balance with Examples from North America and Sequoia National Park. Cornell University, California. In.
Stephenson, N.L., 1990. Climatic control of vegetation distribution: the role of the water balance. Am. Nat. 649–670.
Stephenson, N.L., 1999. Reference conditions for giant sequoia forest restoration: structure, process, and precision. Ecol. Appl. 9, 1253–1265.
Swain, D.L., Horton, D.E., Singh, D., Diffenbaugh, N.S., 2016. Trends in atmospheric patterns conducive to seasonal precipitation and temperature extremes in California. Sci. Adv. 2.
Tardieu, F., Simonneau, T., 1998. Variability among species of stomatal control under fluctuating soil water status and evaporative demand: modelling isohydric and anisohydric behaviours. J. Exp. Bot. 419–432.
Ustin, S.L., Roberts, D.A., Pinzón, J., Jacquemoud, S., Gardner, M., Scheer, G., Castañeda, C.M., Palacios-Orueta, A., 1998. Estimating canopy water content of chaparral shrubs using optical methods. Remote Sens. Environ. 65, 280–291.
York, R.A., Battles, J.J., Eschtruth, A.K., Schurr, F.G., 2011. Giant sequoia (Sequoiadendron giganteum) regeneration in experimental canopy gaps. Restor. Ecol. 19, 14–23.
Young, D.J.N., Stevens, J.T., Earles, J.M., Moore, J., Ellis, A., Jirka, A.L., Latimer, A.M., 2017. Long-term climate and competition explain forest mortality patterns under extreme drought. Ecol. Lett. 20, 78–86.
Zuur, A.F., Ieno, E.N., Elphick, C.S., 2010. A protocol for data exploration to avoid common statistical problems. Methods Ecol. Evolut. 1, 3–14.